Infrared and infrared emission spectroscopic study of China typical kaolinite and halloysite

Hongfei Cheng [a,b,c], Ray L. Frost [c]*, Jing Yang [c], Qinfu Liu[b], Junkai He[b]

[a] School of Mining Engineering, Inner Mongolia University of Science & Technology, Baotou 014010, China

[b] School of Geoscience and Surveying Engineering, China University of Mining & Technology, Beijing 100083, China

[c] Chemistry Discipline, Faculty of Science and Technology, Queensland University of Technology, 2 George Street, GPO Box 2434, Brisbane, Queensland 4001, Australia

* Corresponding author: Chemistry Discipline, Faculty of Science and Technology, Queensland University of Technology, 2 George Street, GPO Box 2434, Brisbane, Queensland 4001, Australia;
Tel: +61 7 3864 2407;
Email: r.frost@qut.edu.au

Abstract: The structure and thermal stability between typical China kaolinite and halloysite were analysed by X-ray diffraction (XRD), infrared spectroscopy, infrared emission spectroscopy (IES) and Raman spectroscopy. Infrared emission spectroscopy over the temperature range of 300 to 700 °C has been used to characterise the thermal decomposition of both kaolinite and halloysite. Halloysite is characterised by two bands in the water bending region at 1629 and 1648 cm^{-1}, attributed to structure water and coordinated water in the interlayer. Well defined hydroxyl stretching bands at around 3695, 3679, 3652 and 3625 cm^{-1} are observed for both kaolinite and halloysite. In the 550 °C infrared emission spectrum of halloysite is similar to that of kaolinite in 650-1350 cm^{-1} region. The infrared emission spectra of halloysite were found to be considerably different to that of kaolinite at lower temperatures. This difference is attributed to the fundamental difference in the structure of the two minerals.

Key words: Infrared; Infrared emission spectra; Raman; Kaolinite; Halloysite

1. Introduction

Interest in the structure and thermal stability of kaolin stems from a number of reasons. Firstly, kaolin has wide applications in industry, particularly used as paper filler, rubber filler and a coating pigment [1-8]. These applications imply the value of the kaolin at present or in future. Interest in such minerals and their thermal stability rests with the possible identification of these minerals and related dehydrated phyllosilicate related mineral [9]. Many studies on differential thermal analysis and application studies of some related minerals have been published [10-13]. Study on their structure and thermal analysis has proven extremely useful for determining the stability of minerals [9, 12, 14-18]. Secondly, kaolin occurrences are common and known on all the continents of the world except Antarctica, but commercially viable deposits are relatively few in number [7, 19]. Kaolin, especially low whiteness kaolin, is important from an environmental point of view. The industrial application of kaolin or China clay are diverse and depend largely on the physical properties, such as whiteness, thermal stability, particle size, etc. specific for each kaolin deposit [20]. However, most of the industrial kaolin in china which generally contain a certain amount of organic carbon must be calcined to improve whiteness [21, 22]. Therefore, it is of high importance to understand well the structure and stability of kaolin.

Kaolin is rock comprised largely of the kaolin group mineral including kaolinite, halloysite, dickite and nacrite. The most common kaolin mineral is kaolinite, which has attracted much attention over a long period of time [8, 23]. The last two members of the kaolin group are relatively rare, although significant deposits of halloysite are known. Kaolinite, $Al_4[Si_4O_{10}](OH)_8$ is a naturally occurring inorganic polymer with a layer structure consisting of siloxane and gibbsite-like layers. The siloxane layer is composed of SiO_4 tetrahedra linked in a hexagonal array. The bases of the tetrahedra are approximately coplanar and the apical oxygen atoms are linked to a second layer containing aluminum ions and OH groups (the gibbsite-type layer). Halloysite in its hydrated form presents the approximate stoichiometry $Al_4[Si_4O_{10}](OH)_8 \cdot 2H_2O$ and basal a spacing near 10.1 Å. This halloysite (10Å) easily dehydrates in atmospheric pressures at temperatures around 60 °C or in vacuum at room temperature. This anhydrous form has a basal spacing near 7.2 Å and is metastable, recovering its interlayer water in the moist environment. The 1:1 layers in hydrated halloysite are separated from each other by a water layer and occur in a scroll-like morphology, halloysite has a larger cation exchange capacity and surface area than kaolinite [18, 24, 25]. Halloysite, unlike kaolinite, its structure is disordered in both the “a” and the “b” crystalline axis directions in successive layers [25]. Because both halloysite and kaolinite are present in kaolin deposits in a wide range of percentages in China, distinguishing these two clay minerals is difficult [26].

Vibrational spectroscopic methods such as infrared (IR) spectroscopy and infrared emission spectroscopy (IES) have been considered as an alternative analytical method because they are facile [27]. Infrared emission spectroscopy has been widely applied to study mineral such as attapulgite and other minerals [28-30]. To date there have been few report of using infrared emission spectroscopy in studying

the thermal stability and differentiation of the kaolin group minerals. Yet infrared emission spectroscopy is such a powerful technique and is seriously underutilized in this regard. In this work, the infrared spectroscopy and infrared emission spectroscopic are used to investigate the structure changes and thermal stability of kaolinite and halloysite.

2. Experimental methods

2.1 Materials

Two kaolin samples, including kaolinite (NSJ-1) and halloysite (XRW-1), were selected for this study (Table 1). Samples were used directly, without prior size fraction separation, since one of the objectives was to determine the influence on the degree of order of the particle size of kaolinite and halloysite.

2.2 X-ray diffraction

X-ray diffraction patterns were collected using a PANalytical X'Pert PRO X-ray diffractometer (radius: 240.0 mm). Incident X-ray radiation was produced from a line focused PW3373/10 Cu X-ray tube, operating at 40 kV and 40 mA, with Cu Kα radiation of 1.540596 Å. The incident beam passed through a 0.04 rad soller slit, a 1/2 ° divergence slit, a 15 mm fixed mask, and a 1 ° fixed antiscatter slit.

2.3 Infrared spectroscopy

Infrared spectra were obtained using a Nicolet Nexus 870 FTIR spectrometer with a smart endurance single bounce diamond ATR cell. Spectra over the 4000-650 cm^{-1} range were obtained by the co-addition of 64 scans with a resolution of 4 cm^{-1} and a mirror velocity of 0.6329 cm/s. Spectra were co-added to improve the signal to noise ratio. No sample preparation was involved.

Band component analysis was undertaken using the Jandel'Peakfit'(Erkrath, Germany) software package which enabled the type of fitting function to be selected and allowed specific parameters to be fixed or varied accordingly. Band fitting was done using a Lorentz-Gauss cross-product function with the minimum number of component bands used for the fitting process. The Lorentz-Gauss ratio was maintained at values greater than 0.7 and fitting was undertaken until reproducible results were obtained with squared correlations (r^2) greater than 0.998. Band fitting of the spectra is quite reliable providing there is some band separation or changes in the spectral profile.

2.4 Infrared emission spectroscopy

FTIR emission spectroscopy was carried out on a Nicolet Nexus 870 FTIR spectrometer, which was modified by replacing the IR source with an emission cell. A description of the cell and principles of the

emission experiment have been published elsewhere [9, 17, 28, 29, 31]. Approximately 0.2mg of kaolin was spread as a thin layer on a 6 mm diameter platinum surface and held in an inert atmosphere within a nitrogen-purged cell during heating. The infrared emission cell consists of a modified atomic absorption graphite rod furnace, which is driven by a thyristor-controlled AC power supply capable of delivering up to 150 A at 12 V. A platinum disk acts as a hot plate to heat kaolin sample and is placed on the graphite rod. An insulated 125 -μm type R thermocouple was embedded inside the platinum plate in such a way that the thermocouple junction was less than 0.2mm below the surface of the platinum. Temperature control of ± 2 °C at the operating temperature of the sample was achieved by using a Eurotherm Model 808 proportional temperature controller, coupled to the thermocouple.

In the normal course of events, three sets of spectra are obtained over the temperature range selected and at the same temperatures; those of the black body radiation, the platinum plate radiation, and the platinum plate covered with the sample. Normally only one set of black body and platinum radiation is required. The emission spectrum at a particular temperature was calculated by subtraction of the single beam spectrum of the platinum backplate from that of the platinum covered with the sample, and the result ratioed to the single beam spectrum of an approximate black body (graphite). This spectral manipulation is carried out after all the spectral data has been collected.

The emission spectra were collected at intervals of 50 °C over the range 100-1000 °C. The time between scans (while the temperature was raised to the next hold point) was approximately 100s. It was considered that this was sufficient time for the heating block and the powdered sample to reach temperature equilibrium. The spectra were acquired by co-addition of 128 scans for the whole temperature range, with an approximate scanning time of 1min, and a nominal resolution of $4cm^{-1}$. Good quality spectra can be obtained providing the sample thickness is not too large. If too large a sample is used then the spectra become difficult to interpret due to the presence of combination and overtone bands. Spectral manipulation such as baseline adjustment, smoothing and normalization was performed using the Spectra calc software package (Galactic Industries Corporation, NH, USA).

2.5 Raman spectroscopy

The crystals of kaolinite or halloysite were placed and oriented on the stage of an Olympus BHSM microscope, equipped with 10× and 50× objectives and part of a Renishaw 1000 Raman microscope system, which also includes a monochromator, a filter system and a charge coupled device (CCD). Raman spectra were excited by a He–Ne laser (633 nm) at a resolution of 2 cm^{-1} in the range between 3500 and 3800 cm^{-1}. Repeated acquisition using the highest magnification was accumulated to improve the signal-tonoise ratio. Spectra were calibrated using the 520.5 cm^{-1} line of a silicon wafer. In order to ensure that the correct spectra are obtained, the incident excitation radiation was scrambled. Spectral manipulation such as baseline adjustment, smoothing and normalisation was performed using the GRAMS® software package (Galactic Industries Corporation, Salem, NH, USA).

3. Results and discussion

3.1 X-ray diffraction (XRD)

The XRD patterns of the kaolinite and halloysite samples together with XRD patterns of the standard minerals are shown in Fig. 1. The XRD patterns of the kaolins show identical patterns to the standards. The halloysite XRD pattern shows a diffraction peak at 2θ=8.82° which is related to (001) plane. This basal reflection of halloysite is due to its tubular morphology, high degree of disorder, small crystal size and interstratifications of layer with various hydrations, but the d-spacing of kaolinite is 7.15 Å at 2θ of 12.34°. The degree of structural disorder of the kaolinite samples can be evaluated on the basis of the XRD background in the range 2θ=20─30°, and the width of the (002) diffraction peak d=3.58 Å at half the maximum height [32-34]. Structural order in the kaolinite was estimated using the Hinckley index (HI) [32], and which is 1.03. The XRD patterns of these two kaolins mineral show quartz impurity. The chemical composition of these two kaolins is reported in Table 2. A comparison of the chemical analysis of the kaolinite and halloysite shows some variation. The chemical composition of SiO_2 is less for halloysite, but LOI (Loss on ignition) is greater than for kaolinite. This variability may be attributed to differences in the geological environment such as the degree of weathering or the extent of transportation of the minerals during formation or deposition [35].

3.2 Infrared spectroscopy (ATR-IR)

The infrared spectra of halloysite and kaolinite in the 3050-3750 cm^{-1} region are shown in Fig.2a. The IR spectra of kaolinite and halloysite in the hydroxyl stretching region show four important features[36-40]: bands are observed at (a) (ν_1) 3695 cm^{-1}, which is attributed to the hydroxyl stretching of the inner surface hydroxyl (b) bands (ν_2) at 3668 cm^{-1} assigned to the out-of-phase vibration of the inner surface hydroxyls (c) bands (ν_3) at 3653 cm^{-1} attributed to the second out-of-phase vibration of the inner surface hydroxyls and (d) bands (ν_5) at 3619 cm^{-1} assigned to the inner hydroxyls. Another six intense bands (ν_6, ν_7, ν_8, ν_9, ν_{10}, ν_{11}) are observed in the region of 3050-3600 cm^{-1}, which are due to the different kinds of water in the structure of halloysite. It is reported that the water in the interlayer of halloysite(10 Å) has been found to occur in two different environments [41]. One type of water (hole water) is keyed into the ditrigonal holes formed by the tetrahedra oxygens and is strongly bonds to the silicate; the other type (associated water) is weakly bonded to the interlayer surfaces. Therefore, the hole water has its stretching vibration bands at (ν_8) 3525 and (ν_9) 3450 cm^{-1} (the exact position of the band seems to depend on the state of hydration), whereas associated water has two broad stretching vibration band at (ν_{10}) 3373 and (ν_{11}) 3251 cm^{-1}. The band observed (ν_7) 3554 cm^{-1} is assigned to the hydrogen bonded between the associated water and the halloysite surface. Another band is observed at (ν_6) 3593 cm^{-1}, which is due to

hydrogen bonded between the hole water and associated water. This hydrogen bond is weak in the structure of halloysite. However, no band is observed in this region in the IR spectrum of kaolinite, which indicates that there is no structural water in kaolinite. Therefore, IR spectroscopy is proved once again to be a powerful technique to characterize the kaolinite and halloysite. The results of the band component analysis of the infrared spectra are reported in Table 3.

Fig. 2b shows the IR spectra of the kaolinite and halloysite in the 650-1850 cm^{-1} region. For the halloysite compared with kaolinite, two infrared bands are observed at (ν_{12})1648 and (ν_{13})1629 cm^{-1} in the halloysite spectrum. The probable assignment of these bands is to the water HOH bending mode. The fact that two bands are observed suggests that there is water present in the halloysite (10Å) structure. This corresponds with the hydroxyl stretching frequencies above. The band at (ν_{12})1648 corresponds to strongly hydrogen bonded water, whereas the band at (ν_{13})1629 cm^{-1} is attributed to non-hydrogen bonded water and corresponds to the position of the water bending mode [28]. These two bands indicate that there is water molecule in the interlayer of halloysite. The (ν_{14})1117 cm^{-1} shoulder is assigned to stretching mode of apical Si-O, while the bands at (ν_{15})1030 and (ν_{19}) 907 cm^{-1} are caused by the stretching vibrations of Si-O-Si and bending modes of Al-O-H, respectively [42, 43]. The other bands at (ν_{20})796 and (ν_{22})746 cm^{-1} are also typical bands of OH translation vibrations of halloysite [42].

The fact that eight bands in the region 3050-3600 cm^{-1} and 1600-1700 cm^{-1} are observed suggests that there are two types of water present in the halloysite structure. This is the main difference between halloysite and kaolinite in the IR spectroscopy. Overall, IR spectra provide greater spectral feature and better spectral resolution to characterize the kaolin group minerals; however, kaolin group minerals usually need calcinations to improve the properties of these minerals. Therefore, the thermal comparison study is also important to analysis the structural change of these mineral in order to improve the industrial application.

3.3 Infrared emission spectroscopy

Typical infrared emission spectra of kaolinite and halloysite are shown in Fig. 3a and b. The spectra clearly show the temperature at which the OH group are lost; in the case of kaolinite is about 650 °C, but in halloysite is about 550 °C. In the 400-600 °C temperature range obvious structure changes are observed. In order to follow these thermal decompositions three spectra at 150, 350 and 550 °C were selected for further analysis. The infrared emission spectra at these temperatures for kaolinite in the 650-1350 cm^{-1} range are shown in Fig. 4a. In the 150 °C spectrum bands are observed at 1203, 1145, 1110, 1058, 995, 914, 800, 784, 757 and 696 cm^{-1}. However, the bands at 1203 and 800 cm^{-1} disappeared in the 350 °C spectrum and the bands at 1145 and 914 cm^{-1} show a small shift to lower wavenumber. In the 550 °C spectrum only four bands at 1195, 1112, 1024 and 782 cm^{-1} are observed. The infrared emission spectra of halloysite at 150, 350 and 550 °C in the 650-1350 cm^{-1} range are shown in Fig.4b. More bands modification occurs for this mineral in this series spectral region. The bands at 1068, 1043, 1004 and 948 cm^{-1} are observed in the

150 °C spectrum, but they are not found in the 350 °C spectrum. A new band at 1179 cm^{-1} is shown in the 350 °C. The band at 800 cm^{-1} in the 150 °C spectrum shift to 838 cm^{-1} in the 350 °C spectrum. The bands at 948 and 1004 cm^{-1} in the 150 °C spectrum at 1028 cm^{-1} in the 350 °C spectrum are ascribed to the OH deformation modes in the layer of halloysite. In the 550 °C spectrum also only four bands at 1195, 1042, 863 and 773 cm^{-1} are observed.

The infrared emission spectra of kaolinite and halloysite in the 3350-3750 cm^{-1} region at 150, 350 and 550 °C are shown in Figs. 5a and b respectively. Five bands are observed for kaolinite at 150 °C at 3614, 1623, 1656, 3683 and 3695 cm^{-1}; at 350 °C only four at 3615, 3625, 3654 and 3683 cm^{-1}. The band at 3695 cm^{-1} is attributed to hydroxyl stretching of the inner surface hydroxyl, which disappeared at 350 °C. The higher wavenumber bands at 3656 and 3683 cm^{-1} (at 150 °C), 3654 and 3683 cm^{-1} (at 350 °C) and 3658 and 3673 cm^{-1} (at 550 °C) are assigned to the OH stretching bands. Similar assignments are made for halloysite. The other bands in these spectra are associated with water stretching vibrations [28, 31]. In the region of 3050-3600 cm^{-1}, six bands are found in the IR spectrum of halloysite as discussed above. However, in the infrared emission spectra at 150 °C, only two bands at 3460 and 3540 cm^{-1} are observed, due to the hole water which retained until 350 °C. The disappeared four bands are related to the associated water which escaped before 150 °C. These two kinds of water lost at different temperatures, which indicate that they have different thermal stability. The associated water leaves first leaving the hole water behind. This finding is in excellent agreement with the work reported by Costanzo and Giese [24].

Considerable differences are found between kaolinite and halloysite of infrared emission spectra data. The dehydration of kaolinite and halloysite is different, which is followed by the loss of the intensity of the water hydroxyl bands. The intensity and position of four hydroxyl-stretching show some differences, especially when the temperature is raised. The bands are observed at 3673, 3658 and 3623 cm^{-1} only in the spectrum of kaolinite at 550 °C and are not observed in this spectrum region of halloysite. These bands illustrate that the temperature of dehydroxylation of kaolinite is much higher than halloysite. In the same time, this evidence can be used to differentiate halloysite from kaolinite. The bands in the 650-1350 cm^{-1} are different between kaolinite and halloysite when temperature is raised. These differences are attributed to the basic structural difference in the two minerals.

3.4 Raman spectroscopy

A number of Raman spectroscopy studies of the hydroxyl of kaolinite have been reported [44-49], but very few in halloysite. Kaolinite is described as having low and high defect structures depending on the stacking of the kaolinite layers. Low defect (ordered) kaolinite have a regular stacking sequence whereas high defect (disordered) kaolinite show disordered stacking. Fig. 6 displays the Raman spectrum of the hydroxyl-stretching region of the low defect kaolinite and halloysite. Raman spectra of the low defect kaolinite have been reported previously [44]. Table 4 reports the band component analysis of the Raman

spectra of the hydroxyl-stretching region of kaolinite and halloysite. The band is observed at (ν_5) 3627 cm^{-1} in halloysite and at 3626 cm^{-1} in kaolinite, which can both be assigned to the vibration of inner hydroxyl. The Raman spectra of kaolinite show differences from halloysite at room temperature (Fig. 6). The band at (ν_6) 3643 cm^{-1}in halloysite is attributed to hydrogen band that the inner surface hydroxyl group bonded to the water in the layer of halloysite. Thus the band at (ν_6) 3669 cm^{-1} disappeared. There is also the possibility that these two hydroxyl stretching bands were shown in the lower wavenumber in halloysite than in kaolinite. A band at (ν_4) 3681 cm^{-1} for halloysite and at (ν_4) 3688 cm^{-1} for kaolinite was observed, which is attributed to the transverse optic vibration of inner surface hydroxyl and is only observed in the crystals with a high aspect ratio. The ν_4 band is not normally observed in infrared spectra but contributes significant intensity in Raman spectra [37].

4. Conclusions

Infrared and infrared emission spectroscopy was used to study the difference in the structure and thermal stability between typical Chinese kaolinite and halloysite. The differences of content and position of water and hydroxyl groups in the kaolinite and halloysite were observed by the IR spectroscopy. Six bands in the region of 3050-3600 cm^{-1} were observed in IR spectrum of halloysite. The difference also was observed in the region of 1600-1700 cm^{-1} of IR spectrum. These difference are mainly because the water in the layer of halloysite. Significant difference was found in the XRD results.

The infrared emission spectra of kaolinite and halloysite showed the changes of hydroxyl stretching and the structure when temperature increased. It is clearly shown that two kinds of water in halloysite are lost in different steps by the infrared emission spectra. The dehydration of hole water in halloysite at around 350 °C and the dehydroxylation of kaolinite at above 550 °C are clearly shown in the infrared emission spectra. The temperature of dehydroxylation of halloysite is at below 550 °C, however the bands of hydroxyl also are also observed at above 550 °C. The hydroxyl stretching frequencies were observed by Raman spectroscopy. These results give us the possibility instructional advice to improve the properties of these minerals in the industrial application, in the same time; these are beneficent to distinguish these two clay minerals. The excellent reproducibility of infrared spectroscopy and the infrared emission spectroscopy technique have made it possible to successfully apply to improve the properties kaolin group minerals and differentiate halloysite from kaolinite.

Acknowledgment

The authors gratefully acknowledge the financial support provided by the National “863” project of China (2008AA06Z109) and infra-structure support of the Queensland University of Technology, Chemistry Discipline,

Faculty of Science and Technology.

References

[1] R.L. Frost, E. Mako, J. Kristof, J.T. Kloprogge, Spectrochim. Acta A: Mol. Biomol. Spectrosc., 58 (2002) 2849-2859.
[2] F. Franco, L.A. Pérez-Maqueda, J.L. Pérez-Rodríguez, J. Colloid Interface Sci., 274 (2004) 107-117.
[3] F. Franco, M.D. Ruiz Cruz, Clay Miner., 39 (2004) 193-205.
[4] F. Franco, L.A. Pérez-Maqueda, J.L. Pérez-Rodr´ıguez, Thermochim. Acta, 404 (2003) 71-79.
[5] F. Franco, J.A. Cecila, L.A. Pérez-Maqueda, J.L. Pérez-Rodríguez, C.S.F. Gomes, Appl. Clay Sci., 35 (2007) 119-127.
[6] G. Rutkai, É. Makó, T. Kristóf, J. Colloid Interface Sci., 334 (2009) 65-69.
[7] H.H. Murray, Appl. Clay Sci., 17 (2000) 207-221.
[8] C. Nkoumbou, A. Njoya, D. Njoya, C. Grosbois, D. Njopwouo, J. Yvon, F. Martin, Appl. Clay Sci., 43 (2009) 118-124.
[9] R. Frost, D. Wain, J. Therm. Anal. Calorim., 91 (2008) 267-274.
[10] G. Meng, Z. Xu, X. Qi, W. Yang, Z. Xie, Gongye Cuihua, 15 (2007) 1-5.
[11] A. Leszczynska, K. Pielichowski, J. Therm. Anal. Calorim., 93 (2008) 677-687.
[12] A.J. Locke, W.N. Martens, R.L. Frost, Thermochim. Acta, 459 (2007) 64-72.
[13] L.K. Joseph, H. Suja, G. Sanjay, S. Sugunan, V.P.N. Nampoori, P. Radhakrishnan, Appl. Clay Sci., 42 (2009) 483-487.
[14] R. Frost, J. Kristóf, E. Horváth, J. Therm. Anal. Calorim., 98 (2009) 423-428.
[15] R. Frost, S. Palmer, J. Kristóf, E. Horváth, J. Therm. Anal. Calorim., 99 (2010) 501-507.
[16] J. Dubois, M. Murat, A. Amroune, X. Carbonneau, R. Gardon, T.S. Kannan, Appl. Clay Sci., 13 (1998) 1-12.
[17] R.L. Frost, M.L. Weier, Thermochim. Acta, 406 (2003) 221-232.
[18] J.E. Gardolinski, H.P.M. Filho, F. Wypych, Quim. Nova., 26 (2003) 30-25.
[19] H.H. Murray, I. Wilson, Clay. Clay Miner., 55 (2007) 644-645.
[20] M.A. Siddiqui, Z. Ahmed, A.A. Saleemi, Appl. Clay Sci., 29 (2005) 55-72.
[21] S.-l. Ding, Q.-f. Liu, M.-z. Wang, Procedia Earth and Planetary Science, 1 (2009) 1024-1028.
[22] Q. Liu, D.A. Spears, Q. Liu, Appl. Clay Sci., 19 (2001) 89-94.
[23] S. Zhao, T. Wang, H. Xu, Y. Guo, Feijinshukuang, 32 (2009) 37-39, 42.
[24] P.M. Costanzo, J. R. F. Giese, Clay. Clay Miner., 33 (1985) 415-423.
[25] K.P. Nicolini, C.R.B. Fukamachi, F. Wypych, A.S. Mangrich, J. Colloid Interface Sci., 338 (2009) 474-479.
[26] E. Joussein, S. Petit, B. Delvaux, Appl. Clay Sci., 35 (2007) 17-24.
[27] H. Chung, M.-S. Ku, J.-S. Lee, Vib. Spectrosc., 20 (1999) 155-163.
[28] R.L. Frost, S. Bahfenne, J. Graham, Spectrochim. Acta A: Mol. Biomol. Spectrosc., 71 (2008) 1610-1616.
[29] R.L. Frost, J.T. Kloprogge, Spectrochim. Acta A: Mol. Biomol. Spectrosc., 55 (1999) 2195-2205.
[30] R.L. Frost, O.B. Locos, H. Ruan, J.T. Kloprogge, Vib. Spectrosc., 27 (2001) 1-13.
[31] R.L. Frost, G.A. Cash, J.T. Kloprogge, Vib. Spectrosc., 16 (1998) 173-184.
[32] D.N. Hinckley, Clay. Clay Miner., 11 (1963) 229-235.
[33] R. Vigil de la Villa, F. Moisés, S.d.R.M. Isabel, V. Iñigo, G. Rosario, Appl. Clay Sci., 36 (2007) 279-286.
[34] C. He, E. Makovicky, B. Osbaeck, Appl. Clay Sci., 9 (1994) 165-187.
[35] C.S. Manju, V.N. Nair, M. Lalithambika, Clay. Clay Miner., 49 (2001) 355-369.
[36] R.L. Frost, J. Kristof, E. Horvath, J.T. Kloprogge, Spectrochim. Acta A: Mol. Biomol. Spectrosc., 56 (2000) 1711-1729.
[37] R.L. Frost, J. Kristof, E. Mako, E. Horvath, Spectrochim. Acta A: Mol. Biomol. Spectrosc., 59 (2003) 1183-1194.
[38] R.L. Frost, J. Kristof, G.N. Paroz, J.T. Kloprogge, J. Colloid Interface Sci., 208 (1998) 216-225.
[39] R.L. Frost, J. Kristof, G.N. Paroz, T.H. Tran, J.T. Kloprogge, J. Colloid Interface Sci., 204 (1998) 227-236.
[40] E. Horváth, J. Kristóf, R.L. Frost, Appl. Spectrosc. Rev., 45 (2010) 130-147.
[41] P.M. Comstanzo, J. R.F.Giese, Clay. Clay Miner., 33 (1985) 415-423.
[42] S. Mellouk, S. Cherifi, M. Sassi, K. Marouf-Khelifa, A. Bengueddach, J. Schott, A. Khelifa, Appl.

306 Clay Sci., 44 (2009) 230-236.
307 [43] Y. Deng, G.N. White, J.B. Dixon, J. Colloid Interface Sci., 250 (2002) 379-393.
308 [44] R.L. Frost, J. Kristof, L. Rintoul, J.T. Kloprogge, Spectrochim. Acta A: Mol. Biomol. Spectrosc., 56
309 (2000) 1681-1691.
310 [45] R.L. Frost, Clay. Clay Miner., 46 (1998) 280-289.
311 [46] R.L. Frost, J. Kristof, J.M. Schmidt, J.T. Kloprogge, Spectrochim. Acta A: Mol. Biomol. Spectrosc., 57
312 (2001) 603-609.
313 [47] R.L. Frost, T. Thu Ha, J. Kristof, Vib.Spectrosc., 13 (1997) 175-186.
314 [48] R.L. Frost, S.J. van der Gaast, Clay Miner., 32 (1997) 471-484.
315 [49] R.L. Frost, S.J. Van Der Gaast, M. Zbik, J.T. Kloprogge, G.N. Paroz, Appl. Clay Sci., 20 (2002)
316 177-187.
317

LIST OF TABLES

Table 1 kaolin samples

Kaolin Sample	Location	Content of Mineral	Impurities
Kaolinite (NSJ-1)	Fujian Nanshan, China	95% kaolinite	Quartz (5%)
Halloysite (XRW-1)	Hunan Xianrenwan, China	93% Halloysite	Quartz (8.1%), Calcite (0.3%), Gibbsite (8.7%)

Table 2 the chemical composition of kaolin samples

Kaolin samples	SiO_2	TiO_2	Al_2O_3	TFe_2O_3	MnO	MgO	CaO	Na_2O	K_2O	P_2O_5	LOI (Loss on ignition)
NSJ-1	45.31	0.36	37.2	0.27	0.001	0.06	0.25	0.02	0.27	0.16	15.26
XRW-1	35.47	0.065	34.51	1.36	0.22	0.81	0.47	0	0.32	0.03	26.69

Table 3 the IR band component analysis of kaolinite and hallosite

SN		ν_{24}	ν_{23}	ν_{22}	ν_{21}	ν_{20}	ν_{19}	ν_{18}	ν_{17}	ν_{16}	ν_{15}	ν_{14}	ν_{13}	ν_{12}	ν_{11}	ν_{10}	ν_{9}	ν_{8}	ν_{7}	ν_{6}	ν_{5}	ν_{3}	ν_{2}	ν_{1}
NSJ-1	Center	675	693	749	780	797	907	937		997	1030	1117									3619	3652	3668	3690
	FWHM	31.8	19.2	29.2	23.9	13.5	36.8	12.9		65.3	14.7	47.5									7.4	25.4	10.7	21.3
	%	1.01	0.98	2.12	1.68	0.77	9.44	0.70		66.05	1.81	4.87									1.68	2.77	0.49	4.53
XRW-1	Center	685		747		791	905	939	970	998	1029	1119	1629	1648	3251	3373	3450	3525	3554	3593	3622	3647	3676	3697
	FWHM	28.0		29.3		35.2	32.7	14.5	13.2	37.9	39.5	19.5	52.1	44.4	175.5	120	82.9	50.8	27.5	56.2	25.1	38.5	35.8	22.6
	%	0.96		1.95		1.70	16.7	0.77	4.51	33.47	16.0	1.30	0.93	0.60	3.43	4.64	4.81	2.70	0.44	1.56	1.03	0.99	0.79	1.27

Table 4 the Raman hydroxyl component analysis of kaolinite and hallosite

	XRW-1			NSJ-1		
	Center	FWHM	%	Center	FWHM	%
ν_5	3627	17.81	47.50	3626	11.07	5.735
ν_6	3643	8.40	3.63			
ν_2	3658	19.91	6.66	3653	16.21	9.88
ν_3				3669	9.65	2.53
ν_4	3681	20.98	12.44	3688	15.17	15.56
ν_1	3700	19.50	29.76	3698	13.98	33.93

LIST OF FIGURES

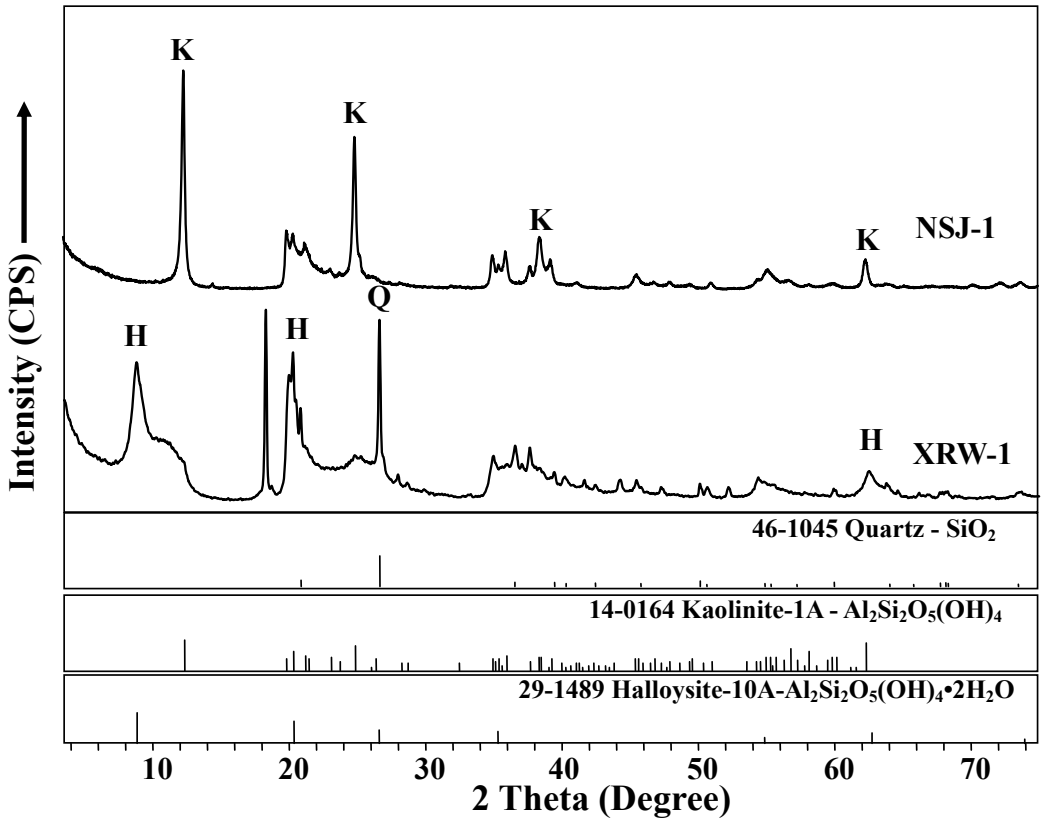

Fig.1 XRD patterns of kaolinite(NSJ-1) and halloysite (XRW-1)

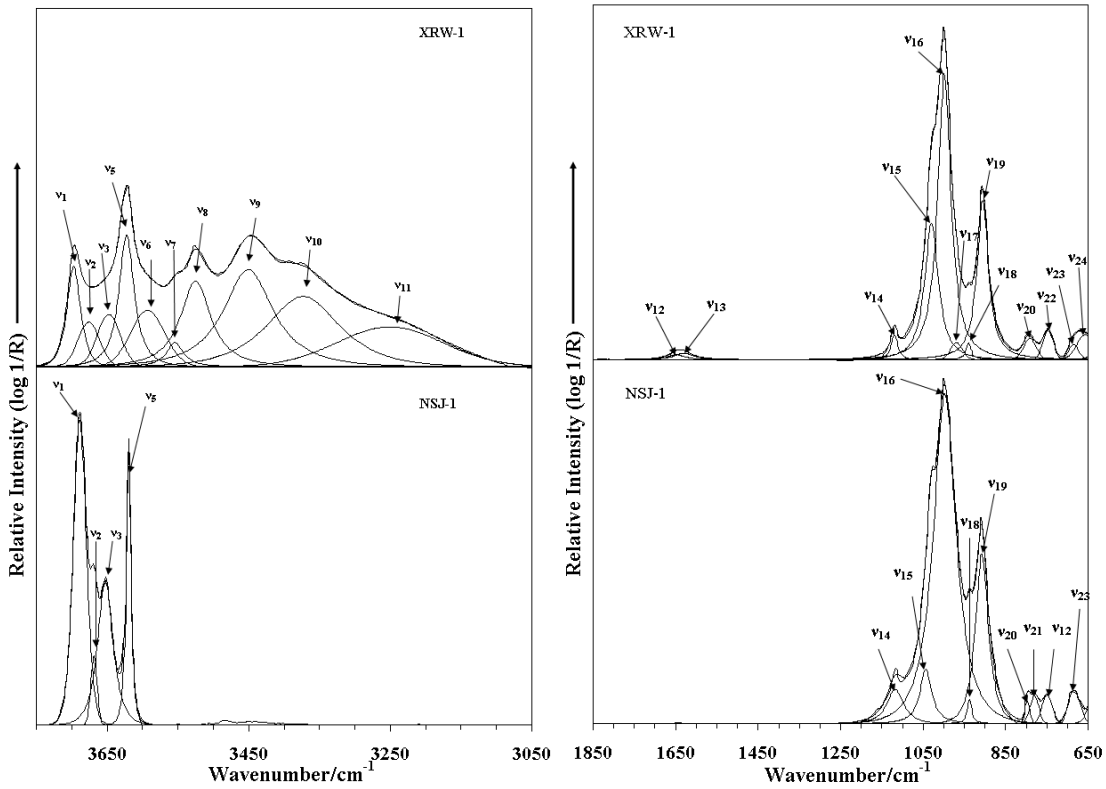

a b

Fig.2 infrared spectra of kaolinite (NSJ-1) and halloysite (XRW-1) (a) in the 3050-3750 cm^{-1} and (b) in the 650-1850 cm^{-1}

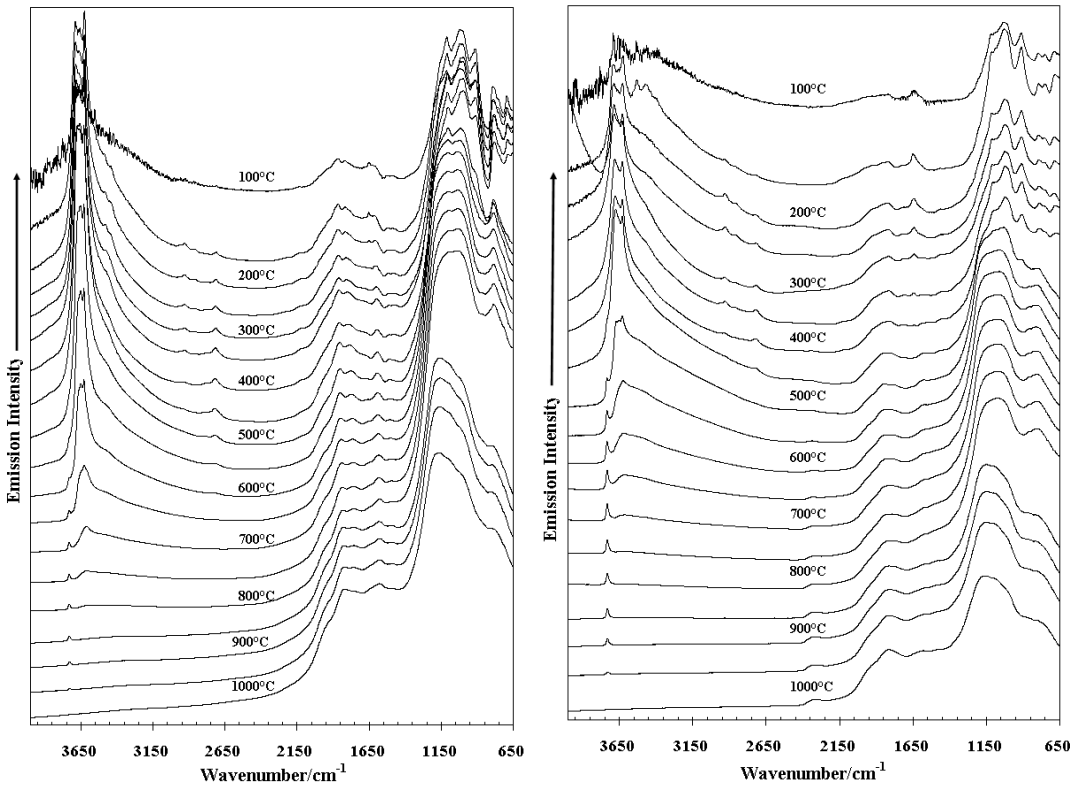

Fig.3 infrared emission spectra of (a) kaolinite (NSJ-1) and (b) halloysite (XRW-1) over the 100-1000 ˚C temperature range

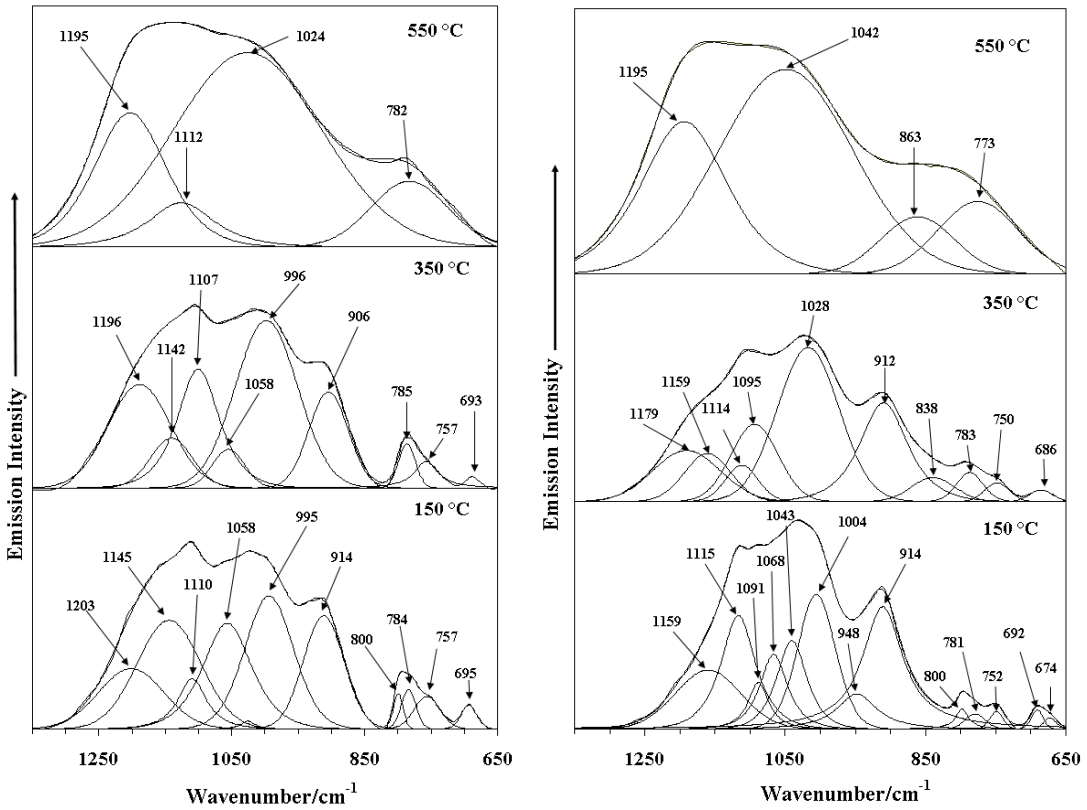

Fig. 4 infrared emission spectra of (a) kaolinite (NSJ-1) and (b) halloysite (XRW-1) in the 650-1350 cm^{-1}

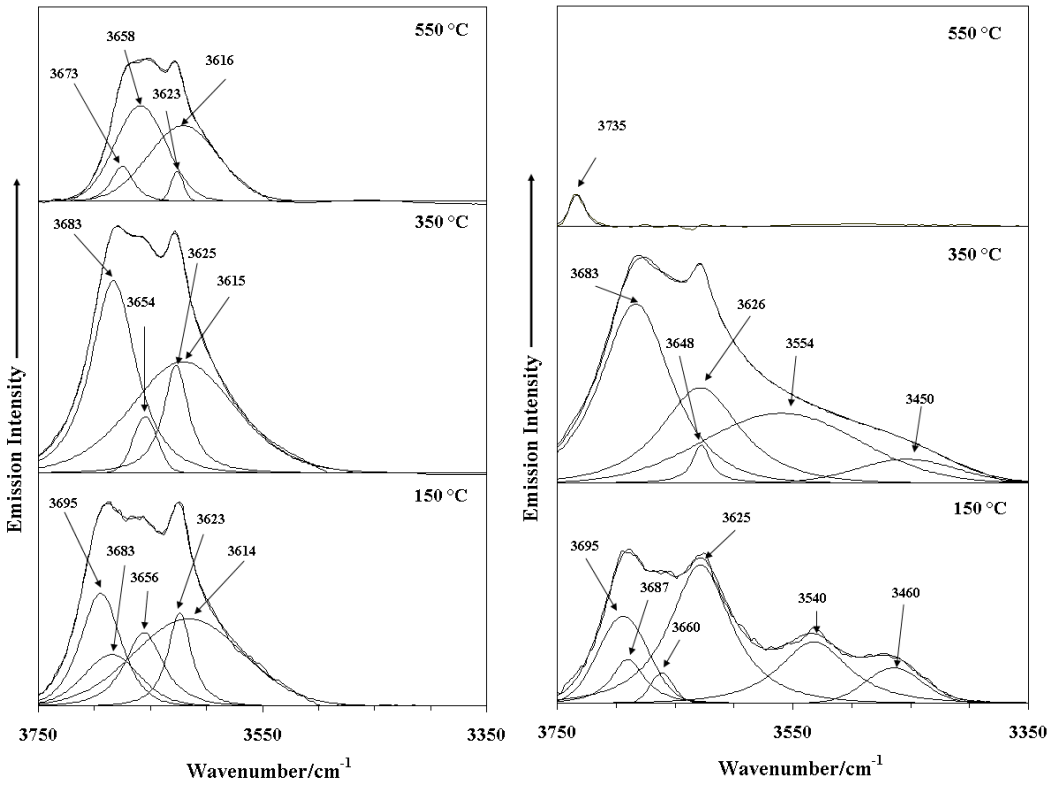

Fig. 5 infrared emission spectra of (a) kaolinite (NSJ-1) and (b)halloysite (XRW-1) in the 3350-3750 cm^{-1}

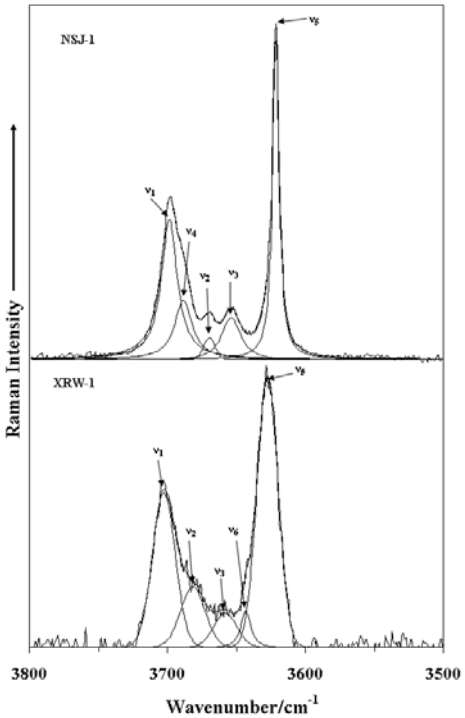

Fig. 6 Raman spectrum of kaolinite and halloysite in the 3500-3800 cm^{-1} region